44. E. Brauer and E. Nann, *Werkst. Korros.*, **25**, 481 (1974).
45. R. Otsuka, *Sci. Papers Phys. Chem. Res.*, **54**, 97 (1960).
46. N. D. Thomashov, V. N. Modestova, L. A. Plavich, and A. B. Averbukh, "Corrosion of Metals and Alloys," Coll. 2, 1965, Israel Program for Scientific Translations, 1966, pp. 66-84.
47. N. T. Thomas and K. Nobe, *Corrosion*, **29**, 188 (1973).
48. F. Mansfeld, *This Journal*, **118**, 1412 (1971).
49. F. Mansfeld, *ibid.*, **120**, 188 (1973).

Pitting Resistance of Cold-Worked Commercial Austenitic Stainless Steels in Solution Simulating Seawater

B. Mazza, P. Pedeferri, D. Sinigaglia, A. Cigada, G. A. Mondora, G. Re, G. Taccani,[1] and D. Wenger[2]

Istituto di Chimica-fisica, Elettrochimica e Metallurgia del Politecnico di Milano, Centro di Studio del CNR sui Processi Elettrodici, 20133 Milano, Italy

ABSTRACT

This paper describes the results of an electrochemical investigation concerning the pitting resistance of cold-worked AISI 304 L and 316 L stainless steels in deaerated 3.5 weight percent (w/o) NaCl solutions of different *p*H's (*p*H = 2, 7, and 9). An anisotropic behavior of specimen surfaces with different orientations to the direction of deformation is shown and discussed in relation to characteristic structural aspects.

A systematic study of the influence of cold plastic deformation on the corrosion behavior of commercial austenitic stainless steels in different aggressive media has been carried out in our laboratory from 1970 onward (1-9), and is now coming to an end.

In this paper, a general view is given of the results concerning the pitting resistance of AISI Types 304 L and 316 L stainless steels cold-worked under various conditions, immersed in deaerated 3.5 w/o NaCl solutions of different *p*H's (*p*H = 2, 7, and 9).

Literature data on pitting corrosion of cold-worked stainless steels are scant and inconsistent (10-16). In particular, the critical pitting potential has been observed either to remain unaffected by cold work, or to shift to more negative values. This inconsistency should not arouse surprise: as a matter of fact, commercial steels are generally considered, and especially after cold plastic deformation their microstructure is neither simple, nor well controlled by the different authors (also in relation to the different working conditions).

[1] Present address: LTM-CNR, Cinisello Balsamo, Milano, Italy.
[2] Present address: CISE, Segrate, Milano, Italy.
Key words: corrosion, pitting, austenitic stainless steels, cold plastic deformation.

Experimental and Materials (Microstructure Analysis)

Materials were first annealed at 1050°C for 1 hr and water quenched (solution heat-treatment), then submitted to cold plastic deformation by either tension, drawing, or rolling, at room temperature (25°C) or at liquid nitrogen temperature (−196°C). Chemical compositions and some structure characteristics of the stainless steels under study (after the solution heat-treatment) are given in Table I. The microstructure analysis of the deformed materials was carried out by means of magnetic measurements, x-ray diffraction, and transmission electron microscopy.

Magnetic measurements (17) enable us to determine (following the scheme of Table II) the weight percentage of ferromagnetic α'-martensite in the deformed steels [the weight percentage of δ-ferrite in the non-deformed state being negligible (see Table III)].

Transmission electron microscopy shows the presence of the following: (*i*) dislocations, with a tendency to their arrangement in a cell structure; (*ii*) deformation bands, which can be resolved either as deformation twins or as ϵ-martensite, and (*iii*) platelets of α'-martensite (approximately one micron in length and

Table I. Chemical compositions and some structure characteristics of the commercial austenitic stainless steels under study (after the solution heat-treatment)

Steel type	Composition (w/o) C	Si	Mn	P	S	Cr	Ni	Mo	Cu	N	ASTM grain-size number[a]	M_{d30}[b] (°C)	M_s[c] (°C)	Subsequent cold-working
AISI 304 L	0.025	0.45	1.39	0.023	0.021	18.60	8.75	0.50	0.24	0.036	6-6.5	+22	<−196	Tension
	0.032	0.54	1.64	0.009	0.009	18.60	8.70	0.48	0.20	0.038	7-7.5	+16	<−196	Drawing
	0.020	0.41	1.40	0.032	0.013	18.10	10.30	0.32	0.24	0.039	4-5	+18	<−196	Rolling
AISI 316 L	0.022	0.43	1.51	0.033	0.023	16.80	10.65	2.90	0.07	0.033	5-5.5	−14	<−196	Tension
	0.023	0.40	1.45	0.034	0.021	16.60	10.90	3.00	0.08	0.037	5.5-6	−17	<−196	Drawing
	0.026	0.41	1.24	0.008	0.011	16.10	10.90	2.20	0.07	0.034	3.5-4.5	+7	<−196	Rolling

[a] Determined according to ASTM Designation E 112.
[b] Temperature at which 50% of martensite is formed in tension after a true strain of 0.30 [calculated according to Ref. (17) and (18)].
[c] Martensite starting temperature.

Table II. Scheme showing how the w/o of ferromagnetic phase (M%) in the deformed austenitic stainless steels under study is determined (17)

σ_H = specific saturation magnetization (emu/g) measured at a given magnetic field strength H (as a rule in our measurements, H = 20,000 oe)

↓

σ_s = specific saturation magnetization (emu/g) corrected for the austenite paramagnetic contribution as follows: $\sigma_s = \sigma_H - 2.5 \times 10^{-5} H$

↓

$100 \times \sigma_s = (M\%) \times \sigma_s^\circ \rightarrow (M\%)$

↑

σ_s° constant calculated for each steel composition as follows (from Angel):

$$\sigma_s^\circ = 160.4 + \Sigma_i \Delta\sigma_i^\circ \times \Delta c_i$$

160.4 = specific saturation magnetization (emu/g) of a totally-martensitic reference heat whose chemical composition (w/o) is as follows (from Angel): C = 0.09; Si = 0.42; Mn = 0.42; Cr = 18.20; Ni = 8.6; Mo = 0.29; N = 0.053

$\Delta\sigma_i^\circ$ = coefficients calculated from Angel's data. His values for each element are as follows: C = 8.34; Si = 3.38; Mn = −0.29; Cr = 2.77; Ni = −0.076; Mo = 0.33; N = 36

Δc_i = difference between the weight percentages of the element "i" in a given steel and in the reference steel.

N.B.: The values of the different magnetic quantities are given in cgs units to allow an easy comparison with data of Ref. (17). Relation between SI units and cgs units is as follows:

Quantity	cgs unit	SI unit	Conversion factor for cgs to SI units
Magnetic field	Oersted (oe)	Ampere turns per meter (A/m)	$\times 10^3/4\pi$
Magnetic moment	emu	Weber meter (Wb m)	$\times 4\pi \cdot 10^{-10}$

a few tenths of a micron in width) at the intersections of the deformation bands; in all three cases the amounts increase with increasing degree of deformation. Dislocations or deformation bands prevail when the steels under study are deformed at room temperature, while deformation bands with platelets of α'-martensite prevail in the case of cold-working at liquid nitrogen temperature (Fig. 1a). In this latter case, the deformation structure at the higher degrees of deformation consists almost solely of small equiaxed grains of α'-martensite (Fig. 1b).

The results of the microstructural investigations are summarized in Table III. The phenomenological aspects previously described in the literature (17-23) are confirmed.

Specimens for the electrochemical experiments were cut so as to obtain different orientations of the surface exposed to the aggressive medium, with respect to the direction of deformation. Longitudinal (L) and transversal (T) surfaces in the cases of tension and drawing, and longitudinal (L), long-transversal (T_L), and short-transversal (T_S) surfaces in the case of rolling were considered.

A detailed description of the procedure for specimen surface preparation of the polarization cell and electrode assembly is given elsewhere (4-7). The testing solution temperature was maintained at 40°C, in order to compare the results with those obtained in a physiological saline solution in previous research work. Nitrogen was continuously bubbled to remove the air. Saturated calomel reference electrodes (SCE) were used.

The currently popular electrochemical techniques, *i.e.*, the cyclic polarization (or electrochemical hystere-

Table III. Results of the microstructural investigations

Steel type	Deformation: Type	Deformation: Temperature (°C)	Deformation: Degree[a] (%)	Vickers hardness number[b]	X-ray diffraction: Phases[c]	Magnetic measurements: Ferromagnetic phase (w/o)	Transmission electron microscopy: Dislocations density ($\times 10^9$ cm/cm^3)	Transmission electron microscopy: Deformation bands[c]	Transmission electron microscopy: α'-martensite[c]	Transmission electron microscopy: Austenite[c]
AISI 304 L	Tension	25	0	147	—	0.3	1.3	—	—	≃100%
			10	202	$\gamma + \alpha'$(v.l.)	0.7	15	l.	n.o.	≃100%
			15	228	$\gamma + \alpha'$(l.)	1.5	>20	m.q.	l.	l.p.
			30	313	$\gamma + \alpha'$(m.q.)	10.6	>20	m.	m.q.	p.
		−196	9	326	$\gamma + \alpha'$(m.q.) + ϵ(v.l.)	37.5	—	m.	m.	m.
			13	415	$\gamma + \alpha'$(m.) + ϵ(v.l.)	66.5	—	l.p.	p.	l.
			19	459	$\gamma + \alpha'$(p.) + ϵ(v.l.)	73.0	—	v.l.	l.p.	n.o.
AISI 316 L		25	0	135	—	0.04	1.2	—	—	100%
			10	198	γ	0.04	10	n.o.	n.o.	100%
			15	220	γ	0.04	>20	l.	n.o.	l.p.
			30	288	γ	0.25	>20	m.q.	n.o.	l.p.
		−196	9	274	$\gamma + \alpha'$(m.q.) + ϵ(v.l.)	18.0	—	m.	m.q.	p.
			13	355	$\gamma + \alpha'$(m.) + ϵ(v.l.)	41.0	—	p.	m.	m.q.
			19	425	$\gamma + \alpha'$(m.) + ϵ(v.l.)	60.0	—	v.l.	p.	l.
AISI 304 L	Drawing	25	0	143	—	0.30	0.90	—	—	≃100%
			10	200	$\gamma + \alpha'$(v.l.)	0.40	30	l.	n.o.	≃100%
			30	292	$\gamma + \alpha'$(m.q.)	9.2	—	m.	m.q.	l.p.
			50	366	$\gamma + \alpha'$(m.)	35.7	—	p.	m.	p.
		−196	10	298	$\gamma + \alpha'$(m.) + ϵ(v.l.)	31.6	—	m.	m.	p.
			30	406	$\gamma + \alpha'$(p.)	78.2	—	v.l.	p.	l.
			50	494	$\gamma + \alpha'$(l.p.)	88.8	—	v.l.	l.p.	n.o.
AISI 316 L		25	0	136	—	0.04	1.0	—	—	100%
			10	192	γ	0.04	20	l.	n.o.	100%
			30	272	γ	0.20	—	m.	v.l.	l.p.
			50	331	γ	1.7	—	l.p.	l.	l.p.
		−196	10	246	$\gamma + \alpha'$(l.)	3.2	—	m.	l.	l.p.
			30	400	$\gamma + \alpha'$(m.q.) + ϵ(v.l.)	54.8	—	v.l.	p.	m.q.
			50	413	$\gamma + \alpha'$(p.)	75.6	—	v.l.	l.p.	l.
AISI 304 L	Rolling	25	0	135	—	0.05	1.0	—	—	100%
			10	203	$\gamma + \alpha'$(v.l.)	0.14	17	m.q.	n.o.	l.p.
			30	272	$\gamma + \alpha'$(v.l.)	0.60	>20	p.	n.o.	l.p.
			50	307	$\gamma + \alpha'$(l.)	2.35	>20	p.	n.o.	l.p.
		−196	10	272	$\gamma + \alpha'$(m.q.) + ϵ(v.l.)	26.2	—	m.	m.q.	p.
			30	417	$\gamma + \alpha'$(p.) + ϵ(v.l.)	63.0	—	p.	m.	m.q.
			50	466	$\gamma + \alpha'$(l.p.) + ϵ(v.l.)	86.5	—	v.l.	l.p.	n.o.
AISI 316 L		25	0	142	—	0.06	1.6	—	—	100%
			10	200	γ	0.06	>20	m.q.	n.o.	100%
			30	280	γ	0.13	—	p.	n.o.	l.p.
			50	327	γ	0.70	—	p.	n.o.	l.p.
		−196	10	260	$\gamma + \alpha'$(m.q.)	26.6	—	m.	m.q.	p.
			30	421	$\gamma + \alpha'$(p.) + ϵ(v.l.)	57.3	—	p.	m.	m.q.
			50	476	$\gamma + \alpha'$(l.p.)	62.6	—	v.l.	l.p.	l.

[a] Quantified as reduction in the cross-sectional area.
[b] Values measured on transversal sections (in the case of rolling long-transversal sections) with respect to the deformation direction.
[c] v.l. = very little (<1%); l. = little (1-10%); m.q. = medium quantity (10-40%); m. = much (40-60%); p. = prevailing (60-80%); l.p. = largely prevailing (>80%); n.o. = not observed.

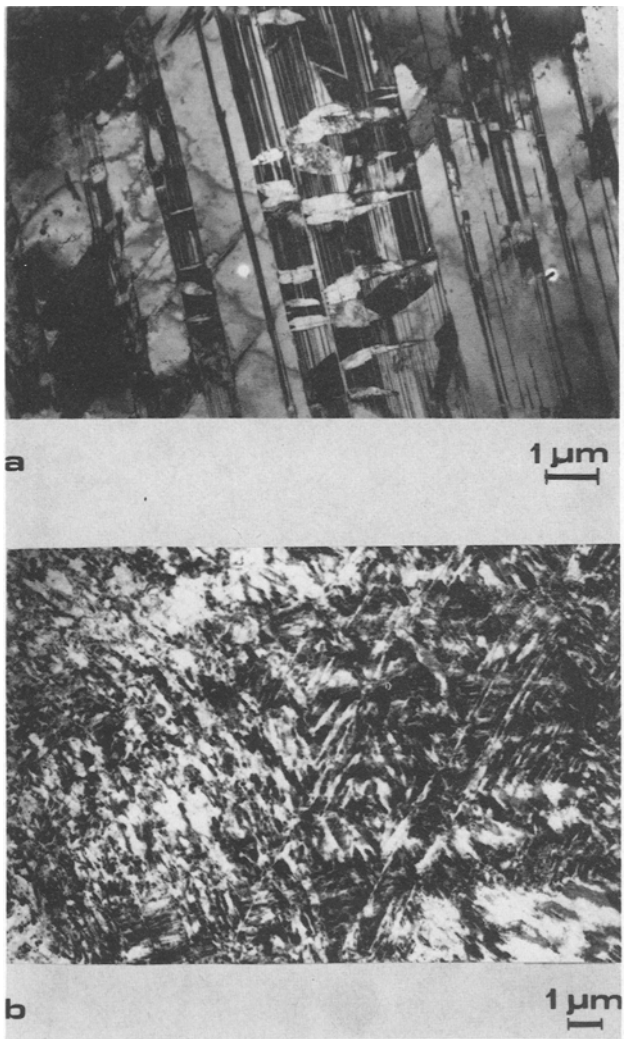

Fig. 1. Deformation structure of AISI Type 304 L stainless steel rolled at liquid nitrogen temperature: (a) deformation degree, 10%; (b) deformation degree, 50%.

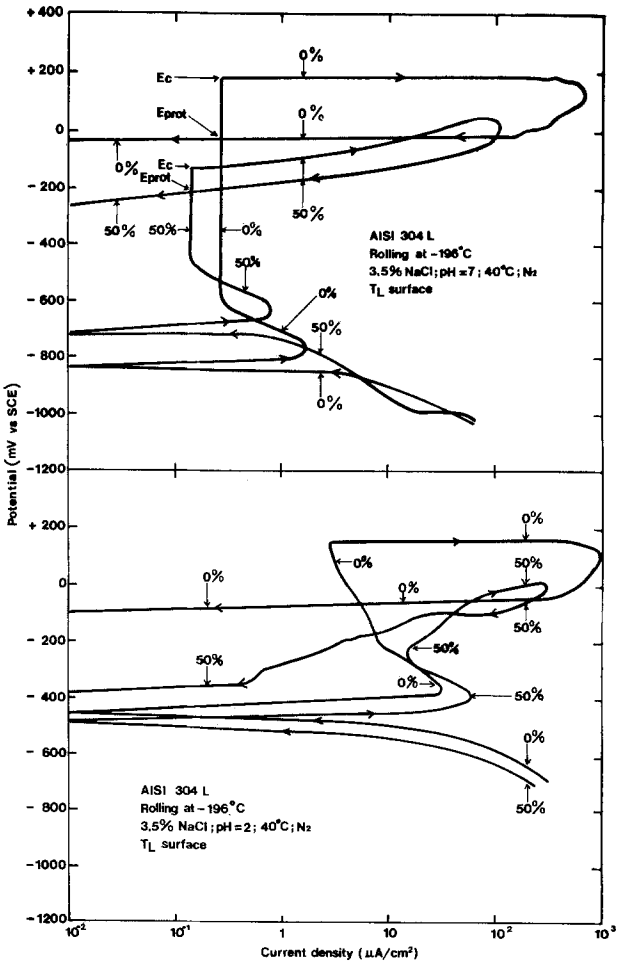

Fig. 2. Cyclic potentiodynamic anodic polarization curves (sweep rate 20 mV/min, sweep reversal current density 100 $\mu A/cm^2$) for AISI Type 304 L stainless steel in deaerated 3.5 w/o NaCl solution at 40°C, indicating the effect of the degree of deformation (0% and 50%) and of the pH (pH = 2 and 7). Deformation by rolling at liquid nitrogen temperature, long-transversal surfaces exposed. Potential values referred to a saturated calomel electrode (SCE). The upper curves show how E_c and E_{prot} values are determined. Cathodic branches of the polarization curves are also reported.

sis) technique (16, 24-29) and the scratch method under potentiostatic conditions (30) were applied for investigating the pitting resistance of the stainless steels under study.

As is well known, cyclic anodic polarization (or electrochemical hysteresis) curves enable us to determine: (*i*) a critical pitting potential (E_c), at which pitting is initiated in the forward scan portion; and (*ii*) a protection potential against pitting (E_{prot}), more active than E_c, at which the growing pits are repassivated in the reverse scan portion. Pitting attack will initiate and propagate if the potential rises above E_c, while new pits will not initiate and existing pits will not propagate if the potential remains below E_{prot}. Inside the hysteresis loop the pitting attack will not initiate, but will propagate if initiated at other potentials. E_c and E_{prot} values were taken from the curves of potential *vs.* logarithm of current density, as shown for example in Fig. 2.[3]

The pitting susceptibility of the stainless steels under study was also tested by means of the scratch method according to the following procedure.[4] The electrode was anodically polarized at a potential value about 200 mV below the critical pitting potential determined by the electrochemical hysteresis technique. Then the specimen surface was scratched with a sapphire point, and the current-time curve was recorded for a few minutes until the scratch repassivated. This procedure was repeated with the electrode potential adjusted in 10 mV steps to more and more noble values, until a critical value E_c was reached at which the scratch failed to repassivate—a failure that was indicated by a gradual rise in current with time.

After the electrochemical tests, the specimens were removed from the assembly and examined under a metallographic microscope.

Results[5]

Both the cyclic polarization and the scratch methods show a decrease in critical pitting potential with increase in the degree of deformation (Fig. 3 and 4). Moreover, an anisotropic behavior of specimen surfaces with different orientations to the direction of deformation should be emphasized. In fact, for every given value of the degree of deformation, E_c decreases when passing from the longitudinal to the transversal surfaces. This anisotropic behavior may be shown also by steels not deformed by cold-work.

The values of E_c obtained by the scratch method are always less noble (with a maximum difference of about 100 mV) and more reproducible than the corre-

[3] The sweep was always reversed at a current density of 100 $\mu A/cm^2$.

[4] Before testing by this method, specimens were prepassivated in a 30 w/o HNO_3 solution at 55°C for 30 min (4-6).

[5] The results shown here refer only to cold-rolling; first, because this is the most widely used operation in the case of austenitic stainless steels, and second, because, for the sake of comparison, tests are in progress on cold-rolled austenitic stainless steels high purity, laboratory produced. Anyway, the results shown for the case of cold-rolling are quite similar to the ones obtained on materials cold-worked by tension or drawing.

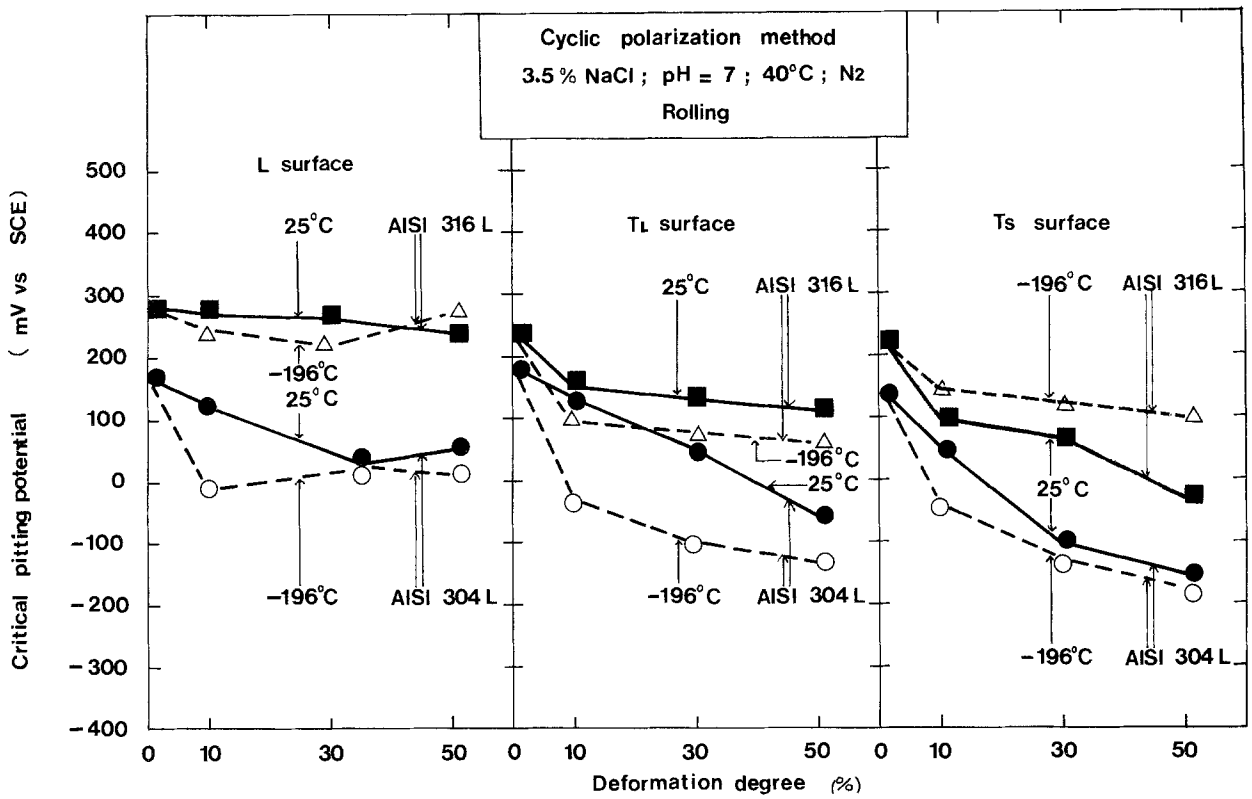

Fig. 3. Critical pitting potential (E_c, determined by the cyclic polarization method, sweep rate 20 mV/min) *vs.* degree of deformation for AISI Type 304 L and 316 L stainless steels deformed by rolling at both room and liquid nitrogen temperatures, and exposed to deaerated 3.5 w/o NaCl solution pH = 7, at 40°C, with different orientations of the specimen surface to the direction of deformation (L = longitudinal, T_L = long-transversal, and T_S = short-transversal surfaces). Potential values referred to a saturated calomel electrode (SCE).

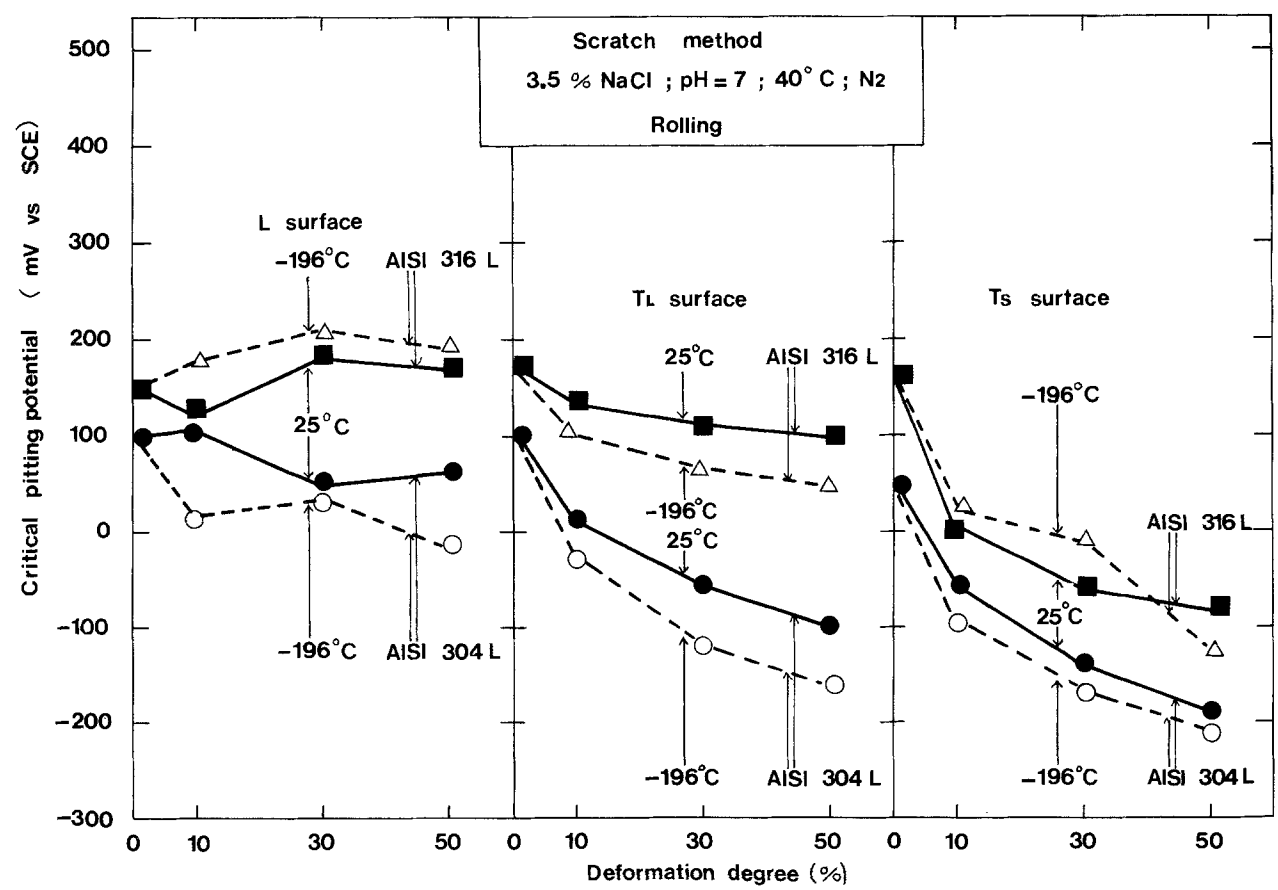

Fig. 4. Critical pitting potential (E_c, determined by the scratch method under potentiostatic conditions) *vs.* degree of deformation for AISI Types 304 L and 316 L stainless steels deformed by rolling at both room and liquid nitrogen temperatures, and exposed to deaerated 3.5 w/o NaCl solution pH = 7, at 40°C, with different orientations of the specimen surface to the direction of deformation (L = longitudinal, T_L = long-transversal, and T_S = short-transversal surfaces). Potential values referred to a saturated calomel electrode (SCE).

sponding values obtained by the cyclic polarization method.

Repassivation of pits in electrochemical hysteresis experiments occurs at potentials E_{prot} which are generally some hundred millivolts less than E_c (no matter how the E_c was obtained) (Fig. 5 and 6). In any case, the protection potential also decreases with increase in the degree of deformation.

On increasing the degree of deformation, especially for the acid pH's and the transversal surfaces, the passivity region and the hysteresis loop in the cyclic polarization curves tend to contract (Fig. 2).

As a whole, the results obtained in 3.5 w/o NaCl solution confirm those obtained in a physiological saline solution in previous research work (4-7).

Microscopic observation shows that the pit shape and general distribution over the specimen surface are unrelated to structural effects of cold plastic deformation such as dislocations, deformation bands, martensite transformation. Moreover, the pit location appears to be unrelated to structural features such as grain boundaries. The results of morphology studies recently described in the literature (15) are thus confirmed.

Discussion

In our opinion, an explanation of the detrimental effect of cold-work on the pitting resistance of the commercial stainless steels under study, and especially of the anisotropic pitting corrosion behavior of the specimen surfaces with different orientations to the direction of deformation, cannot neglect other structural aspects not included among those of the previously given microstructure analysis (*i.e.*, dislocations, deformation bands, and martensite transformation). Thus, the role played by the nonmetallic inclusions through their shape and space distribution should be considered.

It is widely acknowledged that in the case of stainless steels, sulfide inclusions and complex sulfide-oxide or sulfide-silicate inclusions are the most active sites for pit nucleation. Selective dissolution of sulfide inclusions, whether isolated, or surrounding oxide or silicate particles, results in microcavities from which the pit propagation can occur (pitting being thus understood as one kind of crevice corrosion) (14, 31-42).

During plastic deformation, fractures in the inclusions and/or cracks at the inclusion-matrix boundary can occur, mostly due to differences in deformability, with microcavities formation (43, 44).

Moreover, in the deformed state of the steel, the inclusions (which in the as-cast state are spherical and randomly distributed) deform to give triaxial ellipsoids with the major axis on the longitudinal sections (in relation to the direction of deformation) and with the minor axis on the transversal ones (45).

As a result, the transversal sections of the deformed steels show a greater density of inclusions and a geometric shape of the inclusions more favorable to pitting nucleation and propagation than the longitudinal sections (40). Thus, the anisotropic pitting corrosion behavior of deformed steels could remain reasonably explained.

Also, the anisotropic behavior shown by materials not deformed by cold-work could be explained through the influence of factory thermomechanical treatments such as hot-rolling, an influence that is not completely cancelled by the solution heat-treatment.

The presence of α'-martensite (even if it becomes far more prevalent, as shown in Table III for the cold-working at liquid nitrogen temperature) generally

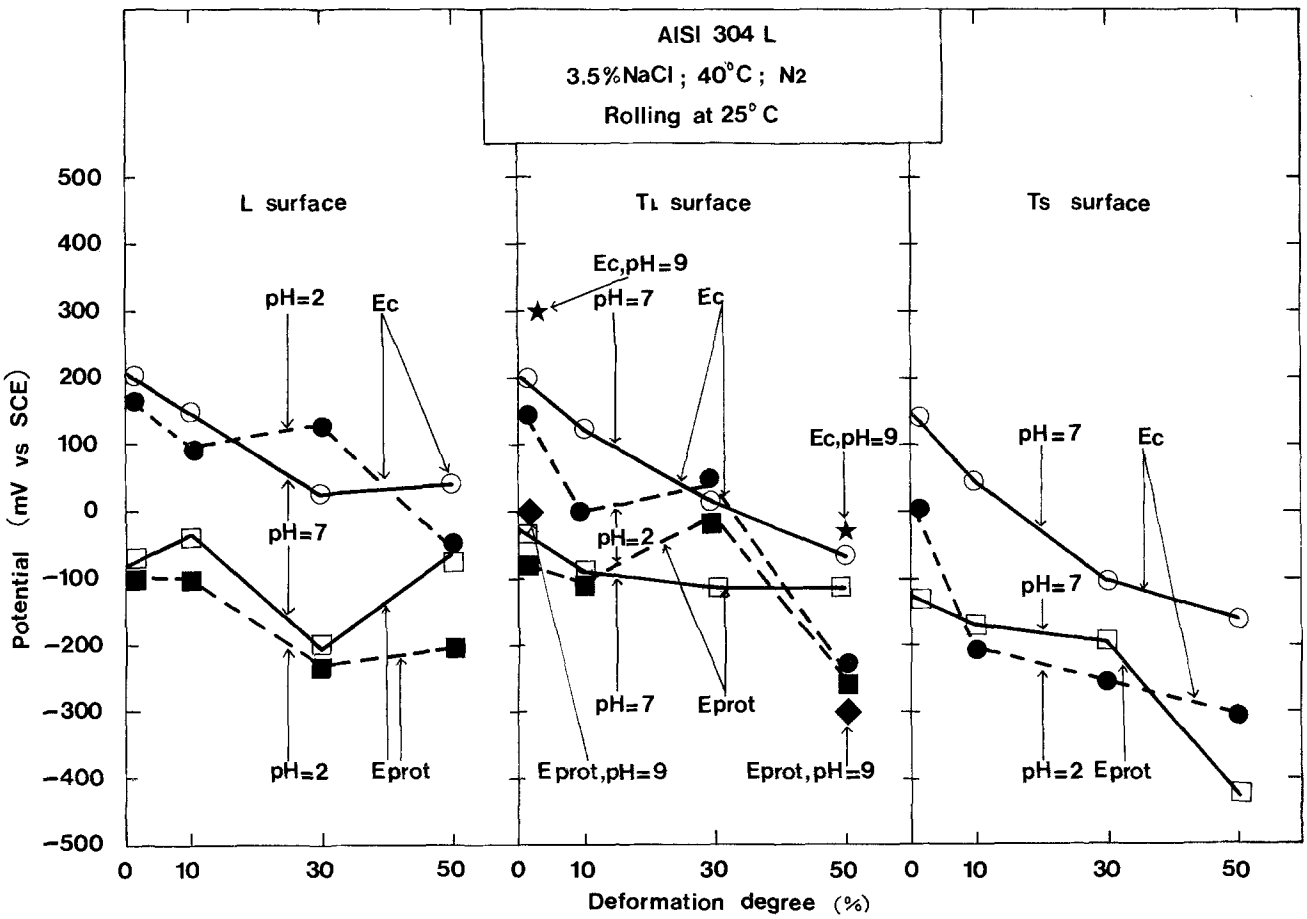

Fig. 5. Critical pitting potential and protection potential against pitting (E_c and E_{prot}, respectively, both obtained by the cyclic polarization method, sweep rate 20 mV/min, sweep reversal current density 100 $\mu A/cm^2$) *vs.* degree of deformation for different orientations of the specimen surface to the direction of deformation (L = longitudinal, T_L = long-transversal, and T_S = short-transversal surfaces), in the case of AISI Type 304 L stainless steel deformed by rolling at room temperature, and exposed to deaerated 3.5 w/o NaCl solutions of different pH's (pH = 2, 7, and 9), at 40°C. Potential values referred to a saturated calomel electrode (SCE).

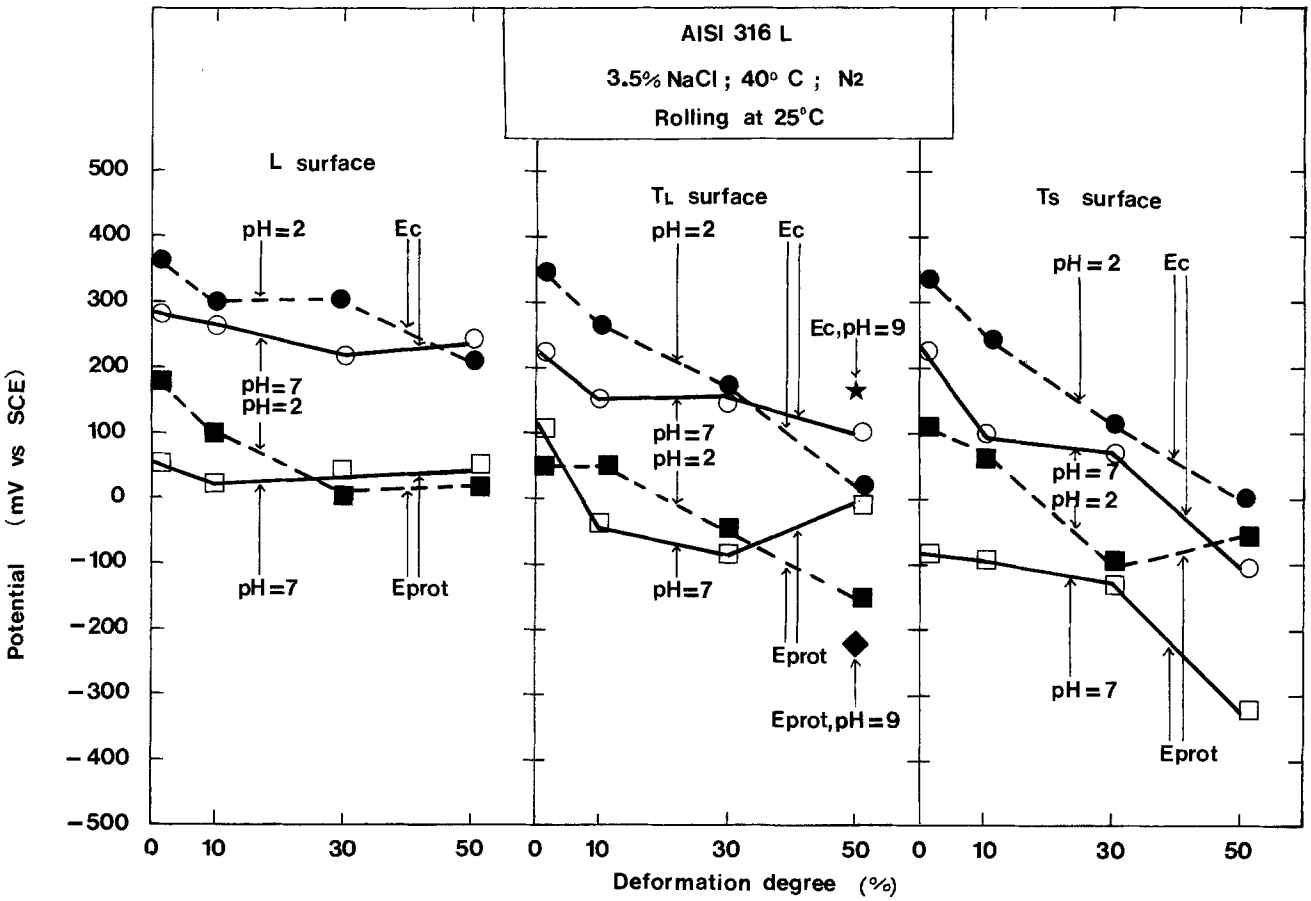

Fig. 6. Critical pitting potential and protection potential against pitting (E_c and E_{prot}, respectively, both obtained by the cyclic polarization method, sweep rate 20 mV/min, sweep reversal current density 100 $\mu A/cm^2$) vs. degree of deformation for different orientations of the specimen surface to the direction of deformation (L = longitudinal, T_L = long-transversal, and T_S = short transversal surfaces), in the case of AISI Type 316 L stainless steel deformed by rolling at room temperature, and exposed to deaerated 3.5 w/o NaCl solutions of different pH's (pH =2, 7, and 9), at 40°C. Potential values referred to a saturated calomel electrode (SCE). In the pH 9 solution, no pitting corrosion has been observed on the undeformed material.

does not seem to produce any significant beneficial effect on pitting resistance of the commercial stainless steels under study (*e.g.*, see the critical pitting potential curves at room temperature and liquid nitrogen temperature in Fig. 3 and 4). This seems to disagree with the results of some authors concerning other types of stainless steel, *e.g.*, the so-called TRIP steels, in which the transformation of austenite to martensite during cold-work at room temperature generally increases the pitting resistance (16).

In order to attain further confirmation of the hypothesis concerning the very important role played by the nonmetallic inclusions, the subsequent step in our research work will be the investigation of the pitting resistance of cold-worked high purity austenitic stainless steels prepared in the laboratory.

Manuscript submitted Feb. 2, 1979; revised manuscript received May 16, 1979.

Any discussion of this paper will appear in a Discussion Section to be published in the June 1980 JOURNAL. All discussions for the June 1980 Discussion Section should be submitted by Feb. 1, 1980.

Publication costs of this article were assisted by the Centro di Studio del CNR sui Processi Elettrodici.

REFERENCES

1. W. Nicodemi, P. Pedeferri, and D. Sinigaglia, *Metallurgia Italiana*, **63**, 23 (1971).
2. D. Sinigaglia, P. Pedeferri, B. Mazza, G. P. Galliani, and L. Lazzari, *ibid.*, **65**, 77 (1973).
3. B. Mazza, P. Pedeferri, D. Sinigaglia, U. Della Sala, and L. Lazzari, *Werkst. Korros.*, **25**, 239 (1974).
4. A. Cigada and P. Pedeferri, *Ann. Chim.*, **65**, 509 (1975).
5. B. Mazza, P. Pedeferri, D. Sinigaglia, A. Cigada, L. Lazzari, G. Re, and D. Wenger, *This Journal*, **123**, 1157 (1976).
6. A. Cigada, B. Mazza, P. Pedeferri, and D. Sinigaglia, *J. Biomed. Mater. Res.*, **11**, 503 (1977).
7. A. Cigada, B. Mazza, G. A. Mondora, P. Pedeferri, G. Re, and D. Sinigaglia, "Corrosion and Degradation of Implant Materials," ASTM STP 684, p. 144, ASTM, Philadelphia. Pa. (1979).
8. B. Mazza, P. Pedeferri, D. Sinigaglia, A. Cigada, G. Fumagalli, and G. Re, *Corros. Sci.*, In press.
9. G. Re, D. Sinigaglia, D. Wenger, and A. Benvenuti, *Metallurgia Italiana*, In press.
10. G. Herbsleb and W. Schwenk, *Stahl Eisen*, **87**, 709 (1967).
11. S. Szklarska-Smialowska and M. Janik-Czachor, *Br. Corros. J.*, **4**, 138 (1969).
12. P. Forchhammer and H. J. Engell, *Werkst. Korros.*, **20**, 1 (1969).
13. A. Randak and F. W. Trautes, *ibid.*, **21**, 97 (1970).
14. S. Szklarska-Smialowska, "Localized Corrosion," NACE-3, p. 312, NACE, Houston, Texas (1974).
15. R. Stefac and F. Franz, *Corros. Sci.*, **18**, 161 (1978).
16. B. C. Syrett and S. S. Wing, *Corrosion*, **34**, 138 (1978).
17. T. Angel, *J. Iron Steel Inst., London*, **177**, 165 (1954).
18. F. C. Hull, *Weld. J. Suppl.*, **52**, 193s (1973).
19. P. M. Kelly and J. Nutting, *J. Iron Steel Inst., London*, **197**, 199 (1961).
20. R. Lagneborg, *Acta Metall.*, **12**, 823 (1964).
21. F. Lecroisey and A. Pineau, *Metall. Trans.*, **3**, 387 (1972).
22. G. Blanc, R. Tricot, and R. Castro, *Mem. Sci. Rev. Metall.*, **70**, 527 (1973).
23. G. B. Olson and M. Cohen, *Metall. Trans.*, **6A**, 791 (1975).

24. B. E. Wilde and E. Williams, *This Journal*, **117**, 775 (1970).
25. B. E. Wilde and E. Williams, *ibid.*, **118**, 1057 (1971).
26. B. E. Wilde and E. Williams, *Electrochim. Acta.*, **16**, 1971 (1971).
27. B. E. Wilde, *Corrosion*, **28**, 283 (1972).
28. M. Pourbaix, L. Klimzack-Mathieiu, C. Mertens, J. Meunier, A. Van Leugenhaghe, L. de Munck, J. Laureys, L. Neelemans, and M. Warzee, *Corros. Sci.*, **3**, 239 (1963).
29. E. D. Verink, Jr. and M. Pourbaix, *Corrosion*, **27**, 495 (1971).
30. N. Pessal and C. Liu, *Electrochim. Acta*, **16**, 1987 (1971).
31. A. Szummer, Z. Szklarska-Smialowska, and M. Janik-Czachor, *Corros. Sci.*, **8**, 833 (1968).
32. M. Smialowski, Z. Szklarska-Smialowska, A. Szummer, and M. Rychcik, *ibid.*, **9**, 123 (1969).
33. Z. Szklarska-Smialowska, A. Szummer, and M. Janik-Czachor, *Br. Corros. J.*, **5**, 159 (1970).
34. G. H. Wagner, A. Desestret, H. Coriou, and L. Grall, *Compt. Rend. Paris*, **270**, Serie C, 1093 (1970).
35. M. Janik-Czachor, A. Szummer, and Z. Szklarska-Smialowska, *Br. Corros. J.*, **7**, 90 (1972).
36. Z. Szklarska-Smialowska, *Corrosion*, **28**, 388 (1972).
37. J. L. Crolet and J. M. Defranoux, *Corros. Sci.*, **13**, 575 (1973).
38. A. Szummer and M. Janik-Czachor, *Br. Corros. J.*, **9**, 216 (1974).
39. P. Poyet, A. Desestret, H. Coriou, and L. Grall, *Mem. Sci. Rev. Metall.*, **72**, 133 (1975).
40. V. Scotto, G. Ventura, and E. Traverso, "The Influence of Non-metallic Inclusion Nature and Shape on Pitting Corrosion Susceptibility of 17Cr-11Ni-2Mo and 18Cr-9Ni Austenitic Stainless Steels," Laboratorio del CNR per la Corrosione Marina dei Metalli, Genova, Italy (1977).
41. I. L. Rosenfeld and I. S. Danilov, *Corros. Sci.*, **7**, 129 (1967).
42. W. D. France, Jr., "Localized Corrosion—Cause of Metal Failure," ASTM STP 516, p. 164, ASTM, Philadelphia, Pa. (1972).
43. S. Rudnik, *J. Iron Steel Inst., London*, **204**, 374 (1966).
44. E. Rozovsky, W. C. Hahn, Jr., and B. Avitzur, *Metall. Trans.*, **4**, 927 (1973).
45. A. Segal and J. A. Charles, *Met. Technol.*, **4**, 177 (1977).

Distribution of Potential Around a Scratch in a Passive Film

P. H. Melville

Central Electricity Research Laboratories, Materials Division, Leatherhead, Surrey, England

ABSTRACT

A Fourier analysis technique has been used to solve the problem of the potential distribution around a long narrow scratch in a passive film on an electrode surface. Analytic solutions have been obtained for situations where linear polarization kinetics may be assumed for the unscratched region, and where the current density is constant over the scratch and very much greater than the current density over unscratched regions. If the half-width l of the scratch is very much smaller than the Wagner polarization parameter for the unscratched region L_c, a simple expression is obtained for the potential distribution close to the scratch. There is a small additional increase in electrode potential at the scratch, but the main increase in potential is over a distance characterized by L_c and not by the size of the scratch. The potential within the electrolyte and along the electrode depends mainly on the logarithm of distance from the center of the crack. There is an angular dependence of the potential only for distances $\lesssim 2l$ from the center of the scratch.

The distribution of potential around coplanar cells consisting of parallel strips of cathode-anode-cathode has been solved by Waber and his associates (1-6) for linear polarization kinetics for a number of different situations. The solutions are obtained in the form of Fourier series for finite systems or as Fourier integrals for infinite ones. More recently a similar method of solution has been extended by Nanis and Kesselman (7), Gal-Or *et al.* (8), and McCafferty (9) for a circular cathode with a concentric central anode. Other problems of practical interest which may be approximated by this kind of model are the distribution of potential around a scratch in a passive film and the distribution of potential around a pit, when the electrode is submerged in a bulk electrolyte. In these systems the anode is very small compared with the cathode, which may be treated as infinite. One dimensional solutions [*e.g.*, Ref. (10)] cannot be used for these systems since they are valid only when the depth of the electrolyte on the surface of the electrode is very much smaller than the width of the anode. As shown below for the case of a scratch analytic solutions may be obtained for the potential distribution, and since for most practical situations the width of the scratch is very much smaller than any of the other dimensions of the system, the solutions reduce to a comparatively simple form (Eq. [42]). The potential around a pit will be considered elsewhere.

It is assumed that quasi steady-state conditions prevail and that there are no appreciable concentration gradients in the electrolyte, so that the problem reduces to the solution of the Laplace equation. These conditions may not be satisfied, if the scratch is repassivated very rapidly. The solutions are also restricted to those conditions where the potential is never very far from the free corrosion potential for the unscratched electrode, so that linear polarization may be assumed. The model may also be applied to other situations with similar geometry, *e.g.*, the distribution of potential around the mouth of a stress corrosion crack.

Mathematical Model

The problem considered is shown in Fig. 1. An infinite plate in the x-y plane at $z = 0$ has a narrow scratch of infinite length and width $2l$ covering the region $-l < x < +l$. This is submerged in an infinite electrolyte. The electrostatic potential $P(x,z)$ in the